Ore Geology Reviews 86 (2017) 526–536

Contents lists available at ScienceDirect

Ore Geology Reviews

journal homepage: www.elsevier.com/locate/oregeo

Critical metals distribution in Tethyan karst bauxite: The cretaceous Italian ores

Giovanni Mongelli [a,*], Maria Boni [b], Giacomo Oggiano [c], Paola Mameli [c], Rosa Sinisi [a], Roberto Buccione [a], Nicola Mondillo [b]

[a] Department of Sciences, University of Basilicata, viale dell'Ateneo Lucano 10, 85100 Potenza, Italy
[b] Dipartimento Scienze della Terra, dell'Ambiente e delle Risorse, University of Naples "Federico II", via Mezzocannone 8, 80134 Naples, Italy
[c] Department of Nature and Land Resources, University of Sassari, via Piandanna 4, 07100 Sassari, Italy

ARTICLE INFO

Article history:
Received 27 January 2017
Accepted 14 March 2017
Available online 16 March 2017

Keywords:
Karst bauxites
Multivariate analysis
Geochemistry
Critical metals
Italy

ABSTRACT

Bauxite is a residual rock, consisting mainly of a mixture of aluminium hydroxides, whose industrial significance is primarily due to its profitably exploitable alumina contents. In the last decades, bauxite, mainly karst bauxite, has been also considered as possible resource of a great number of economically interesting elements including some critical metals such as rare earth elements, Sc, Co, Ni, and Nb. In this study, we present results of univariate and multivariate (R-mode factor analysis) statistics performed on a large data set including chemical composition of the principal Cretaceous karst bauxites from central and southern Italy with the twofold aim to evaluate the inter-elemental relationship among major oxides and critical metals, and describe factors affecting their distribution. Univariate statistics reveal that some critical metals Co, Ni, and LREE, have a significant number of outliers. The Co-Ni relationship associated to the outliers dataset suggests that Co is likely hosted in Ni-rich phases whereas Ce accumulation in authigenic minerals, carbonate-fluoride and phosphate, is at the origin of LREE outliers. Multivariate R-mode statistics, applied to the outliers-devoid database, instead demonstrate that in absence of specific mineralization events, the distribution of most critical metals is controlled by Al-, Fe-, and Ti-oxi-hydroxides and, to a lesser extent, by detrital phases. Among the critical metals, Cr and Y are the exceptions. Their geochemical behaviour seems to be influenced primarily by their own chemical features that are responsible for the mobility of Cr during bauxitization and for the decoupling of Y from the REEs.

1. Introduction

Mineral supplies have become a global concern, especially those used in sophisticated technologies that often affect many aspects of modern life and culture. In 2010, for instance, the unexpected drastic reduction of export quotas for Rare Earth Elements (REEs) from China revealed the vulnerability of a wide range of western high-tech industries. Security of mineral supplies is thus of concern for the European countries and the latest European Union report on critical raw materials listed many critical elements and their possible sources (Herrington, 2013; Mongelli et al., 2016; Vidal et al., 2013). Some of these elements are usually found in bauxite deposits, both of the lateritic and karstic type (Mongelli et al., 2014 and references therein) and, as a consequence the value of bauxite ore might be possibly increased. Significant attention has been recently paid to the processes that control the distribution of several minor elements in these deposits, and to possible extraction techniques (e.g. Abedini and Calagari, 2014; Boni et al., 2013; Buccione et al., 2016; Gamaletsos et al., 2011, 2017; Hanilçi, 2013; Karadağ et al., 2009; Ling et al., 2015; Mameli et al., 2007; Mongelli et al., 2014, 2016; Peh and Kovačević Galović, 2014; Wang et al., 2010; Yu et al., 2014; Yuste et al., 2014, 2017; Zarasvandi et al., 2008). Gallium, for instance, which is a common by-product of Al extraction, ranges in concentrations between <10 and 812 ppm, with an average of 57 ppm in bauxite deposits worldwide (Schulte and Foley, 2013). Bauxites are also considered possible resources of REEs, since up to almost 50% of these elements content may be easily leached using ion exchange agents (e.g. Muchos et al., 2016). In addition, karst bauxite deposits represent the ideal source material for REEs-enriched red mud, which is the remaining waste from the Bayer process that produces alumina from bauxite (Deady et al., 2016). Furthermore, also some other metals included in the European Union report on critical raw materials, such as Sc, Co, Ni, and Nb usually concentrate in bauxite,

* Corresponding author.
E-mail address: giovanni.mongelli@unibas.it (G. Mongelli).

http://dx.doi.org/10.1016/j.oregeorev.2017.03.017
0169-1368/

preferentially in karst bauxite (e.g. Ahmadnejad et al., 2016; Mongelli et al., 2016; Radusinovic et al., 2017).

The distribution of trace elements, as well as the mineralogy and the texture, of karst bauxites in central and southern Italy (Abruzzi, Campania and Apulia regions) and Sardinia have been extensively studied, especially in the last two decades (Mongelli, 1997; Mongelli and Acquafredda, 1999; Mongelli, 2002; Mameli et al., 2007; Mondillo et al., 2011; Boni et al., 2012, 2013; Mongelli et al., 2014, 2015, 2016; Buccione et al., 2016). These studies have generally focused on the genetic model of the deposit and on palaeoclimate and palaeogeographic reconstruction. Italian karst bauxites apart from the Olmedo mine in Sardinia, do not have a particular economic relevance; in any case they can be considered as an analogous of economic bauxite deposits in other parts of the world. An existing regional geochemical data set from these bauxites could be profitably managed using Factor Analysis, thus uncovering hidden multivariate data structures (Reimann et al., 2002).

With this in mind, in this study we used the R-mode Factor analysis, after performing a proper univariate data analysis, on a large geochemical data set derived by Cretaceous karst bauxites distributed across central and southern Italy and northern Sardinia, in order to elucidate: 1- the relationships among the trace metals Sc, V, Cr, Co, Ni, Ga, Y, Nb, and REEs and 2- the factors affecting their distribution.

2. Geological settings

Karstification and bauxite formation require sub-aerial carbonate exposure events. Despite the Italian peninsula bauxites have a well-defined stratigraphic framework, the mechanism that produced the sub-aerial exposure of the carbonate platform, promoting their formation, has remained controversial for a long time. Mindszenty et al. (1995) hypothesized that a lithospheric bulge, induced by the early phases of orogenic collision, was responsible for a long Cretaceous exposure of some sectors of the Southern Apennines and of the Apulian Foreland. Schettino and Turco (2011) hypothesized the occurrence of a Cretaceous to Cenozoic E-W, left-lateral, strike-slip fault crossing southern Italy, which should have induced the uplift of the carbonate platforms and its sub-aerial exposure during Upper Cretaceous in the Apulia and Campania regions (Fig. 1, Table 1). Handy et al. (2010) and Tavani et al. (2013, 2015) evidenced that the Apennine Carbonate Platform was subject to Middle Cretaceous extensional tectonics, possibly promoting the formation of horst and graben and creating uplifted areas favorable to karst bauxite formation.

The Sardinia karst bauxite (Nurra district, NW Sardinia) is hosted within the South European Mesozoic carbonate platform (Fig. 1, Table 1). In Sardinia, most of the Post-Variscan covers cap a low grade metamorphic basement. From Late Permian to Oligocene, NW Sardinia (i.e. Nurra) experienced the same Mesozoic events as other areas of southern stable Europe facing the oncoming Ligure–Piemontese oceanic domain. In this tectonically active still domain, shallow marine sedimentation, including evaporites, characterises a first sequence, which embraces a Ladinian to Albian time span. The first tectonic activity affecting the Mesozoic carbonate shelf occurred during the Middle Cretaceous related to the so-called Bedoulian movements (Combes et al., 1993). This is recognized as low-angle angular unconformities, including a bauxite-bearing stratigraphic hiatus between the Aptian and Coniacian.

2.1. The Apulian karst bauxites

The structure of the Apulia region is affected by the Apenninic (NW–SE trending) and anti-Apenninic (NE–SW-trending) tectonic deformation that divided the region into three main structural blocks: Gargano promontory, Murge area and Salento Peninsula (Funiciello et al., 1991). This region, which is usually called the "Apulian foreland" or "Southern Apennine foreland", represents an extensive foreland domain of the both Apenninic and Dinaric orogens (Spalluto, 2012). Carbonate deposition was frequently punctuated by ephemeral sub-aerial exposures. The early tectonic deformation of the carbonate platform in this area produced two major regional intra-Cretaceous unconformities, characterized by long-lasting sub-aerial exposures (Albian-Cenomanian and Turonian) (Mindszenty et al., 1995). The Murge and Gargano karst bauxite deposits were formed during the Late Cretaceous exposure events, while the allochthonous reworked Salento-type bauxite was deposited on heavily weathered Upper Cretaceous limestones and covered by an Upper Oligocene succession (Esu and Girotti, 2010).

The Murge bauxite (Cenomanian-Turonian) occurs as infills of wide and deep karst cavities bordered by steep walls and is classified as "canyon-like" bauxite (Bárdossy, 1982). These deposits are structurally controlled by pre-existing fault systems, which likely promoted also the accumulation of bauxite. The process started with clay accumulation at the bottom of the karst cavities, followed by "in situ" bauxitization and by the late formation of iron-rich concretions in a water-unsaturated pedogenic environment (Mongelli, 2002).

The Gargano promontory bauxite (Cenomanian-Senonian) occurs as lenticular, irregular bodies on the karstified limestone.

Fig. 1. Simplified present-day tectonic sketch of the Italian peninsula and Sardinia island where the main subduction zones are shown. The insets (a) and (b) display the geological maps of central-southern Italy and Sardinia respectively, including localization of sampled bauxite ores. Each deposit is indicated by the identification label used throughout the text.

Table 1
Main geological and mineralogical features of the central and southern Italy bauxites. Med. = Mediterranean type bauxite; Sal. = Salento-type bauxite; auto. = autochthonous deposit; allo. = allochthonous deposit; ± = accessory mineral phase.

Region of Italy	Typical occurrence	Subset label	Age of deposition	Bauxite type	Texture	Mineralogical assemblage	References
APULIA	Gargano	SGR	Cenomanian/ Turonian	Med., auto.	Massive	Boehmite, hematite, kaolinite, anatase, ±zircon	Bárdossy et al., 1977; Buccione et al., 2016; this study
	Murge	BS	Cenomanian/ late Turonian	Med., auto.	Oolitic, massive	Boehmite, Al-hematite, kaolinite, anatase, ±goethite; ±rutile; ±zircon, ±parisite	Bárdossy et al., 1977; Mongelli et al., 2014
	Salento	OT	Campanian	Sal., allo.	Oolitic	Boehmite, Al-hematite, goethite, anatase, ±rutile	Bárdossy et al., 1977; Mongelli et al., 2016
CAMPANIA	Matese district	GR	Albian/late Turonian-Senonian	Med., auto.	Pisolitic, oolitic	Boehmite, hematite, kaolinite, anatase, ±goethite, ±zircon, ±rutile, ±monazite, ±xenotime, ±apatite, ±ilmenite, ±titanomagnetite, ±gibbsite	Bárdossy et al., 1977; Carannante et al., 1987; Boni et al., 2013
	Caserta district	CS	Albian-Aptian/ Cenomanian	Med., auto.	Massive, oolitic	Boehmite, hematite, kaolinite, illite/montmorillonite, anatase, ±goethite ±zircon, ±monazite, ±gibbsite	Crescenti and Vighi, 1970; Bárdossy et al., 1977; Mondillo et al., 2011
ABRUZZI	Orsello Mt.	AB	Cenomanian	Med., auto.	Massive, oolitic	Boehmite, hematite, kaolinite, goethite, anatase, rutile, ±zircon, ±monazite, ±parisite	Bárdossy et al., 1977; Mondillo et al., 2016; this study
SARDINIA	Nurra district	SN	Aptian/Albian	Med., auto./allo.	Massive, oolitic	Boehmite, kaolinite, goethite, anatase, ±illite, ±rutile, ±bastnasite, ±quartz, ±hematite, ±pyrite, ±zircon	Mameli et al., 2007

This deposit was exploited underground until the seventies of the last century.

The Salento-type deposits mostly consist of hard rounded bauxite pebbles, derived from the erosion, transport and re-deposition of older bauxite from a dismantled middle Campanian deposit (Mongelli et al., 2015).

2.2. The Campania karst bauxites

The karst bauxites of the Campania region (Matese Mountains and Caserta district) are located within the thick Meso-Cenozoic carbonate succession, which builds great part of the Matese and of the Mt. Maggiore mountain chains (Carannante et al., 2009). The palaeogeographic evolution of the Apennine Carbonate Platform in the area is punctuated by several stratigraphic gaps, which are more abundant during Upper Cretaceous (Carannante et al., 2009). In the Matese Mts. the gap extends from Middle-Upper Albian to Turonian-Lower Coniacian (Crescenti and Vighi, 1964), while in the Caserta district the gap is more limited, covering the transition between Albian and Cenomanian. The bauxite bodies form flat, contiguous lenses of a few meters in thickness overlying the Upper Cretaceous karstified bedrock (Bárdossy et al., 1977).

2.3. The Abruzzi karst bauxites

The bauxite district in the Abruzzi region, located in the central sector of the Apennine Carbonate Platform, comprises several deposits situated in the Campo Felice, Monte Orsello and Monti D'Ocre areas. Two main bauxite horizons can be recognized in the platform carbonates: a first corresponding to a Late Albian-Early Cenomanian stratigraphic gap, and a second bounded by Upper Cenomanian-Lower Turonian limestones (Bárdossy et al., 1977; Chiocchini et al., 1994). The most prominent deposits occur along the lowermost of the mentioned gaps. These bauxites form large lenses up to 10 m thick and more than 50 m wide, and were the first to be exploited in Italy.

2.4. The Sardinia karst bauxite

In Sardinia the formation of karst bauxite followed the emersion of the Mesozoic carbonate shelf in Middle Cretaceous. The uplift is related to a transpressional dynamic between the European and the Iberian plates (Oggiano et al., 1987; Combes, 1990). The bauxite unconformably rests on bedrocks, which are different in age and composition. The composition of the bedrock controls the geometry as well as the profile alteration of deposits. True karst and lens-shaped bauxite bodies are common on limestones with Urgonian and Titonian facies as well as on Kimmeridgian and Oxfordian dolostone. Conversely, the bauxite laying on marlstone with Purbeckian facies undertakes an uninterrupted stratiform geometry with a typical vertical profile enriched in kaolinite at the base. These features make such a deposit unique among the Mediterranean bauxites: i.e. the Sardinia type (Combes, 1990) or Type 1 (Mameli et al., 2007). On the bauxite lays a transgressive sequence consisting of Hippurites-bearing limestones followed by marls that spans a Coniacian to Maastrichtian interval.

3. Materials and methods

Fifty-seven samples of Apulian karst bauxites (twenty-two Murge bauxite samples, hereinafter referred to as BS subset, Mongelli et al., 2014; fifteen Gargano bauxite samples, hereinafter referred to as SGR subset, unpublished data; twenty Salento-type bauxite, hereinafter referred to as OT subset, Mongelli et al., 2016), twenty-four samples of Campania karst bauxites (twelve Matese district samples, hereinafter referred to as GR subset; Mondillo et al., 2011; twelve Caserta district samples, hereinafter referred to as CS subset, Mondillo et al., 2011), fifteen samples of the Sardinia karst bauxite (hereinafter referred to as SN subset, Mameli et al., 2007), and six samples of the Abruzzi karst bauxite (hereinafter referred to as AB subset, Mondillo et al., 2016) have been considered for this study.

The composition of the Apulia karst bauxite was determined by ICP and ICP-MS at Activation Laboratories (Ancaster, Canada). The powdered samples were digested using a four acid attack (HF, $HClO_4$, HNO_3, and HCl). In detail, a 0.25-g sample was firstly digested using hydrofluoric acid, then with a mixture of nitric and perchloric acids, before being heated in several ramping and holding cycles using precise programmer-controlled heating that took the samples to incipient dryness. At incipient dryness point, sample residues were re-dissolved in aqua regia and analyzed using Varian ICP and PerkinElmer Sciex ELAN 9000 ICP-MS instruments. Total loss on ignition (LOI) was gravimetrically estimated after overnight heating at 950 °C.

The Campania and Abruzzi karst bauxites were analyzed at the ACME Analytical Laboratories Ltd (Vancouver, Canada). Major oxi-

des and several minor elements were analyzed by ICP-OES following a $LiBO_2/Li_2B_4O_7$ fusion and dilute nitric digestion. Loss on ignition (LOI) derives by weight difference after ignition at 1000 °C. Rare earth and refractory elements were determined by ICP-MS following a $LiBO_2/Li_2B_4O_7$ fusion and nitric acid digestion. In addition, a separate volume split was digested in aqua regia and analyzed by ICP-MS to detect the precious and base metals.

The major elements and V, Ni, Y, and Nb contents of Sardinia karst bauxite were determined by XRF on powder pellets, whereas the Sc, Cr, Co, Ga, and REEs contents were obtained by INAA at Activation Laboratories (Ancaster, Canada). Total loss on ignition (LOI) was gravimetrically estimated after overnight heating at 950 °C.

For all the subsets the certified analytical uncertainties are less than ±5% barring elements at concentrations of ≤10 ppm, which have uncertainties of ±5–10%, except for the elements determined by INAA which have average errors in the ±5% to ±20% range.

4. Results and discussion

4.1. Mineralogical composition and texture

In the bulk bauxitic rock boehmite is the most abundant mineral phase, generally followed by hematite and/or goethite (commonly occurring as Al-rich hematite and goethite), kaolinite, and anatase (Table 1) (Bárdossy et al., 1977). Gibbsite, diaspore, illite, montmorillonite and rutile may occur in some bauxite samples. Among the accessory minerals detrital zircon is the most abundant; monazite, xenotime, titanomagnetite and ilmenite have been also commonly detected. In some cases REE-bearing minerals of the bastnäsite group and secondary LREE-rich phosphates are observed as well (Boni et al., 2013).

Karst bauxites from peninsular Italy and Sardinia share the same texture, which consists in agglomerates of sub-spheroidal concretions (ooids), disseminated in a clayey, locally Fe-rich matrix (Bárdossy et al., 1977; Boni et al., 2013; Mongelli et al., 2014, 2016; Mondillo et al., 2011). Detrital fragments of lateritic crusts and of previously deposited bauxite are generally common, especially in the Campania bauxites. The ooids are composed, in the majority of the cases, of either an Al-hematite or Al-goethite core, followed by concentric layers of alternated Al-hematite/Al-goethite and boehmite. Kaolinite occurs in the matrix only, whereas anatase is contained in both ooids and matrix. Within this frame the exceptions are: i) the Salento-type bauxite where the ooids abundance is much lower than in other Italian bauxites, and their usual texture consists of a large boehmite core surrounded by a thin Al-hematite rim (Mongelli et al., 2015; Buccione et al., 2016); ii) the Type 1 Sardinian bauxite with a profile dominated by white aphanitic bauxite, is devoid of Fe-bearing ooids and characterized by sporadic light grey boehmitic ooliths (Mameli et al., 2007).

4.2. The relationships among the major oxides

Table 2 shows the chemical compositions of the examined bauxite samples divided into the different subsets. The distribution of the major elements reveals, in addition to the expected high Al_2O_3 concentrations, also relevant SiO_2, TiO_2, and Fe_2O_3 contents.

A positive relationship is always observed, across the different subsets, between Al_2O_3 and TiO_2 (Fig. 2), thus demonstrating that titanium accumulates during bauxitization according to its low solubility in the supracrustal environment. In some cases (SGR: $r = 0.96$, $p < 0.01$, CS: $r = 0.97$, $p < 0.01$, GR: $r = 0.89$, $p < 0.01$, and SN: $r = 0.89$, $p < 0.01$) this relationship is highly significant.

A broad negative relationship is observed between Al_2O_3 and SiO_2 (Fig. 2), with the exception of the AB subset ($n = 6$). The highest significances are associated to the SGR ($r = -0.80$, $p < 0.01$), CS ($r = -0.77$, $p < 0.01$), and SN ($r = -0.92$, $p < 0.01$) subsets. The almost general negative correlation between aluminium and silica across the karst bauxite subsets supports the observation that during bauxitization Al minerals mostly form at the expense of silicate phases (Mongelli et al., 2014 and references therein).

Finally, also the relationship between Al_2O_3 and Fe_2O_3 is broadly negative with the exceptions of the SGR and SN subsets (Fig. 2). This inverse correlation is highly significant in the OT subset only ($r = -0.91$, $p < 0.01$). In the karst bauxite from peninsular Italy and Sardinia iron oxi-hydroxides largely occur in the ooids and form as a result of migration and accumulation towards smaller pores in kaolinite-rich zones during the ferrolysis stage of oxidation–hydrolysis process (Mongelli et al., 2014, 2016, and references therein). The iron migration and its accumulation as oxi-hydroxides does not require low water activity conditions as those necessary for Al (boehmite) accumulation which, in turn, means that iron concentrates in bauxite under wetter climates than those promoting the Al enrichment. This explains the observed Al_2O_3-Fe_2O_3 inverse correlation, although the iron redox chemistry may complicate this general trend as probably occurs in the SGR and SN subsets.

4.3. Descriptive statistics and outliers

The box and whisker plots (Fig. 3), in addition to minimum, maximum and median also depict the first and third quartiles and the outliers for each variable. The outliers' identification has been performed by means of the p-values based Grubbs' test, or Extreme Studentized Deviate test. P-values quantify the probability of obtaining a statistic as unusual or more unusual than that observed in the sample, if the null hypothesis were true. If the p-value is small enough, the null hypothesis can be rejected, since the sample would have been an extremely rare event. In our case we defined the "significance level" as "small enough" when p-value is <0.05.

It has to be stressed that the outliers have to be properly evaluated because they contain important information about data quality and unexpected behaviour in the region of interest and may be indicative of specific mineralisation events. Further, the outliers can have a severe influence on factor analysis and they should be removed prior to entering the calculation (Reimann et al., 2002).

Among the major oxides only TiO_2 has a limited variability (median = 2.79, min = 0.71, max = 5.45, std = 0.97) and no outliers. SiO_2 (median = 4.85, min = 0.44, max = 43.58, std = 9.21), Al_2O_3 (median = 52.57, min = 15.52, max = 75.73, std = 9.77), and Fe_2O_3 (median = 20.19, min = 1.45, max = 40.84, std = 7.60) have a larger variability and several outliers. Especially SiO_2 has seven outliers, all belonging to the silica-rich SN subset. In this subset many samples are kaolinite-rich probably as a result of a low temperature hydrothermal silicification along joints and faults (Mameli et al., 2007).

As for the critical metals V (median = 405, min = 141, max = 877, std = 157), Cr (median = 545, min = 141, max = 124, std = 269), and Ni (median = 200, min = 60, max = 1072, std = 166) have the highest variability and V and especially Ni have outliers; most of the Ni outliers belong to the BS subset although the maximum value is observed in one sample from the CS subset. Sc (median = 54.5, min = 16, max = 110, std = 14.4), Co (median = 36.9, min = 5.3, max = 349, std = 40.7), Ga (median = 59.6, min = 16, max = 110, std = 11.9), Y (median = 55.5, min = 25, max = 143, std = 18.4), and Nb (median = 71, min = 14.5, max = 129, std = 26.4) show lower dispersion. Co has the highest number of outliers ($n = 12$) whereas Nb, similarly to TiO_2, has no outliers. Among the REEs, and due to its redox chemistry, the Ce dispersion (median = 213, min = 24, max = 1470, std = 200) affect

Table 2
Concentrations of principal major oxides (wt.%) and critical raw material elements (including trace metals and rare earth elements, ppm) of the southern Italy and Sardinia bauxites.

Sampling site		Major oxides			Critical raw materials (CRMs)																								
		SiO_2 (wt.%)	Al_2O_3	Fe_2O_3	TiO_2 (ppm)	V	Cr	Co	Nb	Ni	Y	Sc	Ga	La (ppm)	Ce	Pr	Nd	Sm	Eu	Gd	Tb	Dy	Ho	Er	Tm	Yb	Lu	ΣREE	LREE	HREE
APULIA	MURGE – BS subset[1]	20.51	44.42	13.18	3.42	381	700	35	88	280	29	44	53	31.8	54.3	7.7	27.1	6.1	1.5	5.2	1.0	6.3	1.4	3.9	0.7	4.6	0.7	152.2	127.0	25.3
		12.13	42.23	25.57	4.41	715	840	28	115	420	25	39	57	43.1	50.9	8.2	28.3	5.4	1.4	4.5	0.9	5.6	1.2	3.7	0.6	3.9	0.6	158.2	135.9	22.4
		10.89	50.1	20.41	4.49	474	810	38	122	480	30	48	68	53.9	192.0	10.2	34.9	6.9	1.7	6.5	1.1	6.5	1.3	4.0	0.7	4.5	0.7	324.8	297.9	27.0
		9.46	49.28	21.78	4.52	522	810	39	121	**500**	33	55	65	58.0	259.0	11.1	38.6	7.5	1.8	7.1	1.2	7.0	1.5	4.2	0.7	5.0	0.7	403.4	374.2	29.2
		10.25	50.1	20.98	4.45	520	830	41	120	**590**	32	55	66	58.2	215.0	11.7	41.0	8.0	2.0	7.5	1.2	7.3	1.5	4.6	0.8	4.8	0.7	364.2	333.9	30.4
		9.57	47.15	23.78	4.59	579	830	40	120	470	34	58	63	63.5	233.0	12.6	43.3	8.7	2.1	7.8	1.3	7.7	1.6	4.6	0.7	5.2	0.8	392.9	361.1	31.8
		10.47	49.93	20.42	4.49	493	790	37	123	480	33	56	63	58.3	153.0	11.8	40.2	8.3	2.0	6.7	1.2	7.7	1.6	4.5	0.8	5.1	0.8	302.0	271.6	30.4
		8.69	47.14	25.31	4.46	522	790	42	119	470	38	65	80	80.0	276.0	17.9	63.9	12.4	2.9	9.8	1.7	9.6	1.9	5.5	0.9	6.2	0.9	489.6	450.2	39.4
		7.49	44.82	28.06	4.46	560	800	41	125	450	47	70	81	168.0	234.0	44.0	149.0	27.4	6.1	16.0	2.5	14.8	2.7	7.4	1.2	8.1	1.1	682.3	622.4	59.9
		8.5	48.76	21.62	4.53	502	830	38	124	**510**	44	59	68	110.0	230.0	25.2	91.3	17.9	4.4	13.6	2.2	12.6	2.5	6.9	1.1	7.2	1.1	526.0	474.4	51.6
		11.28	50	19.62	4.49	453	870	36	110	440	48	54	64	113.0	561.0	28.5	104.0	20.3	5.2	17.9	2.6	13.8	2.5	6.9	1.1	7.2	1.0	884.9	826.8	58.2
		6.79	58.46	13.22	4.54	479	610	**94**	112	450	66	61	**94**	83.1	136.0	20.6	80.3	18.1	4.6	17.0	2.9	17.0	3.2	9.4	1.5	10.1	1.5	405.3	338.1	67.2
		14.66	46.32	21.03	4.06	465	740	37	107	490	46	54	67	108.0	142.0	23.7	85.4	16.9	4.4	14.0	2.2	12.5	2.4	6.6	1.1	6.5	1.0	426.6	376.0	50.7
		14.42	46.25	20.24	4.19	447	740	45	107	480	48	53	61	144.0	240.0	36.1	131.0	23.5	5.5	16.3	2.4	13.3	2.4	6.8	1.0	6.7	1.0	630.0	574.6	55.4
		18.89	44.18	16.87	3.94	378	660	39	101	430	39	49	56	83.7	57.5	19.3	70.3	14.1	3.5	10.4	1.8	10.3	1.9	5.5	0.9	5.9	0.9	285.9	244.9	41.1
		19.44	40.86	20.41	3.86	438	800	46	106	420	42	52	58	115.0	163.0	29.1	107.0	21.4	5.0	14.6	2.3	13.2	2.4	6.5	1.1	7.0	1.0	488.6	435.5	53.1
		17.63	39.38	26.04	4.06	505	860	38	113	410	45	60	60	117.0	**831.0**	29.2	106.0	22.3	5.4	19.1	2.7	14.8	2.7	7.4	1.1	7.6	1.1	**1167.4**	**1105.5**	61.9
		12.74	44.09	24.38	4.26	488	920	37	121	380	46	58	67	93.0	143.0	22.9	84.1	16.6	4.1	12.1	2.0	11.3	2.2	6.1	1.0	6.4	0.9	405.6	359.6	46.1
		15.03	43.92	22.65	4.51	429	850	43	129	480	47	55	68	84.7	133.0	20.0	73.9	14.8	3.7	11.2	1.9	10.9	2.1	5.8	0.9	6.2	0.9	370.0	326.4	43.6
		10.22	53.93	17.2	4.17	405	500	43	103	440	56	58	66	105.0	193.0	23.0	84.1	16.9	3.8	12.9	2.2	13.6	2.6	7.4	1.2	8.0	1.2	474.8	422.0	52.9
		12.77	50.65	19.34	4.02	436	490	**165**	97	**530**	59	60	61	116.0	237.0	26.1	95.0	18.8	4.3	14.8	2.5	14.8	2.8	8.0	1.3	8.6	1.2	551.2	492.9	58.3
		12.58	49.49	20.43	3.78	413	520	46	97	480	55	57	63	118.0	378.0	30.0	109.0	21.1	4.7	15.4	2.5	14.0	2.7	7.4	1.2	7.9	1.1	713.0	656.1	56.9
	SALENTO – OT subset[2]	0.96	56.82	21.57	2.48	223	1060	37	70	150	52	45	56	99.1	157.0	16.0	57.8	11.0	2.4	8.5	1.6	9.4	1.9	5.8	1.0	6.5	0.9	378.9	340.9	38.0
		0.95	57.58	20.7	2.83	207	1010	35	74	160	53	43	58	84.5	123.0	13.7	48.7	9.7	2.1	7.9	1.3	8.5	1.8	5.5	0.9	6.2	0.9	314.7	279.6	35.1
		0.44	59.7	18.01	2.8	196	920	**136**	80	310	57	43	67	84.3	152.0	14.7	53.3	10.7	2.3	8.6	1.6	9.5	2.0	6.1	1.0	6.5	1.0	353.6	315.0	38.6
		1.1	54.5	23.74	2.49	239	930	56	71	190	60	53	52	129.0	204.0	20.2	71.5	13.8	2.9	10.5	1.8	10.6	2.2	6.6	1.1	6.9	1.1	482.2	438.5	43.7
		0.96	54.67	23.8	2.49	222	960	42	69	170	56	48	52	111.0	163.0	17.3	63.5	11.4	2.4	8.7	1.5	9.5	2.0	5.9	1.0	6.4	0.9	404.5	366.2	38.3
		0.9	57.59	21.47	2.59	209	1040	32	73	140	55	44	54	97.5	161.0	15.7	55.5	11.2	2.4	8.6	1.5	8.7	2.0	5.7	1.0	6.1	0.9	377.7	340.9	36.9
		0.92	58.8	19.34	2.85	192	1020	47	78	180	52	43	60	81.7	132.0	13.5	49.1	10.1	2.1	7.8	1.4	8.5	1.9	5.8	1.0	6.5	0.9	322.3	286.4	35.9
		0.9	59.62	19.34	2.96	189	1020	43	80	190	54	43	60	79.0	130.0	13.1	48.8	9.4	2.2	7.7	1.4	8.5	1.8	5.7	1.0	6.3	0.9	315.7	280.3	35.5
		0.85	62.13	16.77	2.96	183	940	**142**	80	290	56	41	57	77.2	147.0	13.1	50.0	10.0	2.1	7.8	1.4	9.3	1.9	5.6	1.0	6.7	1.0	334.1	297.3	36.8
		0.92	58.47	19.91	2.56	196	1110	34	77	170	53	43	60	86.6	135.0	14.4	51.7	10.5	2.3	8.3	1.5	9.3	1.9	5.7	0.9	6.1	0.9	335.1	298.2	36.9
		0.56	58.84	20.1	2.59	219	1020	36	78	220	57	44	68	96.4	146.0	16.3	59.4	11.2	2.4	8.9	1.5	9.5	2.0	6.0	1.0	6.7	0.9	368.3	329.3	38.9
		0.86	58.68	20.13	2.63	201	980	32	74	150	53	44	54	91.8	141.0	14.3	51.2	9.9	2.1	7.7	1.5	8.5	1.8	5.5	0.9	6.2	0.9	343.3	308.2	35.1
		0.86	58.73	20.03	2.57	190	1000	39	77	170	53	42	57	96.7	148.0	15.3	54.6	10.4	2.3	8.1	1.5	9.0	2.0	5.6	1.0	6.4	0.9	361.9	325.0	36.8
		0.89	58.17	20.79	2.61	215	960	**79**	75	210	54	45	53	91.6	156.0	14.4	53.6	10.1	2.1	8.1	1.5	8.7	1.9	5.5	0.9	6.4	0.9	361.7	325.7	36.0
		0.84	59.13	18.07	2.73	188	920	61	74	190	52	42	53	79.3	139.0	12.9	46.6	9.3	1.9	7.3	1.3	8.1	1.7	5.3	0.9	5.8	0.8	320.2	287.1	33.1
		0.94	58.47	21.14	2.69	203	1070	34	76	170	56	46	58	93.6	134.0	14.7	53.1	10.9	2.3	8.6	1.5	9.1	1.9	5.7	1.0	6.5	0.9	343.8	306.3	37.5
		0.95	59.15	20.14	2.72	195	1050	34	80	160	55	44	59	86.4	126.0	13.3	51.1	9.9	2.3	8.6	1.4	8.6	1.9	5.6	1.0	6.1	0.9	323.1	286.7	36.4
		0.91	56.94	23.36	2.45	219	1130	41	71	170	61	50	55	108.0	143.0	17.3	61.8	12.0	2.5	9.7	1.6	9.8	1.9	5.9	1.0	6.6	0.9	382.0	342.1	39.9
		0.45	61.16	19.07	2.54	219	930	31	71	210	56	45	67	117.0	145.0	18.3	65.2	12.2	2.5	9.7	1.7	9.4	1.9	6.1	1.0	6.4	0.9	397.3	357.7	39.6
		0.48	58.81	19.25	2.46	222	920	32	74	210	57	45	67	127.0	152.0	19.8	70.0	12.3	2.6	10.0	1.7	9.9	2.0	6.1	1.0	6.5	1.0	421.9	381.1	40.8
	GARGANO – SGR subset[3]	2.1	56.85	21.08	5.286	382	540	26	100	200	46	68	69	93.8	232	23.3	85.8	17.2	4.08	12.8	2.1	12.9	2.4	7.3	1.11	8	1.18	503.97	452.1	51.9
		2.04	56.25	21.47	5.196	390	580	26	96	200	46	67	69	103	239	26.3	96.8	19	4.56	14.2	2.4	13.8	2.6	7.7	1.15	8.3	1.26	540.07	484.1	56.0
		1.94	57.39	19.81	5.267	384	540	27	100	210	45	65	70	85.3	405	20.7	74.3	14.8	3.52	11.7	2	11.7	2.3	6.9	1.07	7.3	1.11	647.7	600.1	47.6
		3.83	52.04	18.07	4.168	323	420	24	83	190	55	61	61	104	333	27.2	102	20.2	4.91	16.9	2.5	14.6	2.7	7.8	1.17	7.8	1.13	645.91	586.4	59.5
		2.21	56.1	21.29	5.033	401	510	30	102	210	47	73	68	92.5	276	22.3	82.1	16.8	3.99	13.1	2.2	13.1	2.5	7.6	1.13	8.1	1.23	542.65	489.7	53.0
		1.15	54.75	24.52	5.403	499	650	32	107	230	35	68	68	85.6	**634**	18.1	61.2	12.1	2.83	9	1.6	9.5	1.9	5.6	0.88	6	0.92	849.23	811.0	38.2
		1.06	55.67	23.66	5.449	485	630	31	102	240	35	65	68	81.7	556	17	58.3	11.4	2.63	8.9	1.5	9.2	1.8	5.5	0.85	5.8	0.9	761.48	724.4	37.1
		2.58	51.51	21.13	4.519	405	500	49	97	240	47	62	61	94.8	353	21.5	77	14.9	3.58	12.2	1.9	10.9	2.1	6	0.92	6.1	0.87	605.77	561.2	44.6
		2.82	38.71	12.27	2.49	232	350	17	61	170	54	43	43	73.5	210	19.8	74.2	15.7	3.87	13.4	2.1	12.1	2.3	6.7	0.98	6.5	0.97	442.12	393.2	48.9
		3.42	44.69	15.75	2.787	301	420	19	73	200	53	47	53	96.9	351	25.8	92.8	19.7	4.57	15.7	2.3	13.6	2.5	7.2	1.06	7.2	1.09	641.42	586.2	55.2

Table 2 (*continued*)

Sampling site		Major oxides (wt.%)			Critical raw materials (CRMs) (ppm)								La (ppm)	Ce	Pr	Nd	Sm	Eu	Gd	Tb	Dy	Ho	Er	Tm	Yb	Lu	ΣREE	LREE	HREE
		SiO_2	Al_2O_3	Fe_2O_3	TiO_2	V	Cr	Co	Nb	Ni	Y	Sc	Ga																
		4.58	41.29	15.1	2.598	284	370	17	67	180	57	45	45	90.5	225	23.1	84.6	17.2	4.12	14.4	2.2	12.5	2.3	6.6	0.95	6.4	0.95	490.82	440.4	50.4
		3.76	40.33	20.65	2.456	331	400	21	68	180	52	55	47	102	273	25.8	96.2	19.3	4.58	16	2.4	13.5	2.5	7	1.05	6.5	0.97	570.8	516.3	54.5
		4.46	27.51	11.91	1.81	193	320	12	46	150	70	35	31	97.6	259	25	92.8	19.4	4.8	17.1	2.5	14	2.6	7	1.01	6.2	0.9	549.91	493.8	56.1
		4.05	38.86	15.41	2.422	260	360	17	61	180	64	47	44	109	295	29.2	108	22.4	5.24	18.2	2.7	14.4	2.7	7.6	1.09	7.2	1.05	623.78	563.6	60.2
		3.61	36.23	20.3	2.387	332	440	20	64	180	63	51	46	117	296	30	111	22.4	5.39	19.1	2.8	15.6	2.9	8.1	1.17	7.3	1.15	639.91	576.4	63.5
CAMPANIA	MATESE – GR subset[4]	11.21	52.59	14.69	2.40	349	293	38	49	243	48	71	51	308.5	**712.6**	51.7	155.2	16.9	3.1	14.4	2.0	10.1	2.0	6.2	1.1	7.2	1.1	**1292.2**	**1245.0**	47.2
		6.86	63.00	9.99	3.05	411	294	19	62	163	57	61	60	67.1	131.6	16.4	62.1	11.4	2.4	10.4	1.9	10.7	2.2	6.8	1.2	8.2	1.3	333.5	288.6	45.0
		7.15	62.18	10.84	2.76	428	328	22	54	174	58	76	61	79.9	155.0	18.5	69.1	12.9	2.6	11.2	1.9	11.1	2.3	7.1	1.2	7.8	1.3	381.9	335.3	46.5
		7.26	58.63	17.39	2.96	411	440	23	56	174	64	75	56	87.7	154.1	19.8	74.2	13.4	2.9	12.0	2.1	11.9	2.5	7.7	1.3	8.4	1.3	399.2	349.2	50.0
		6.52	62.98	11.60	3.31	452	421	22	65	154	62	74	72	66.7	220.7	17.9	67.4	12.8	2.6	11.6	1.9	11.4	2.3	7.1	1.2	7.9	1.2	432.6	385.5	47.1
		8.05	50.50	26.01	2.48	363	462	22	49	159	79	**110**	57	108.7	**693.1**	32.8	129.1	27.0	5.9	27.1	4.0	20.6	3.8	10.3	1.7	10.9	1.7	**1076.5**	**990.7**	85.9
		10.96	54.68	14.72	2.67	411	321	40	56	246	52	76	54	354.7	**828.1**	55.3	151.0	15.7	2.7	14.6	2.0	11.3	2.2	6.6	1.1	7.8	1.2	**1454.4**	**1404.8**	49.5
		3.82	67.52	10.48	3.38	431	346	18	65	82	55	37	61	45.1	104.8	11.0	42.7	7.9	1.7	7.9	1.5	9.4	2.1	6.1	1.1	7.0	1.1	249.3	211.5	37.8
		3.69	62.50	16.93	3.06	397	398	19	60	93	52	38	60	52.1	115.1	13.5	51.3	10.4	2.2	9.4	1.7	9.8	2.1	6.3	1.1	7.3	1.1	283.3	242.3	41.0
		4.37	64.34	14.34	3.06	397	352	27	62	103	50	35	59	45.3	90.6	11.0	46.0	8.5	1.8	8.2	1.5	9.3	1.9	5.9	1.0	6.6	1.0	238.7	201.3	37.3
		1.54	46.03	**38.95**	2.50	513	342	33	48	126	59	85	50	107.2	232.4	24.6	89.0	16.6	3.5	13.7	2.3	12.9	2.4	6.9	1.2	7.5	1.1	521.3	469.7	51.6
		1.66	48.57	35.39	2.55	499	282	32	49	132	61	75	50	106.0	278.3	24.1	92.4	16.9	3.6	14.6	2.4	13.0	2.6	7.9	1.3	7.9	1.2	572.2	517.7	54.5
	CASERTA – CS subset[5]	9.13	36.75	**37.97**	2.01	411	732	33	36	143	52	36	49	102.0	231.4	27.2	101.8	17.7	3.6	14.5	2.1	10.8	1.9	5.3	0.8	5.4	0.8	525.3	480.1	45.2
		10.01	**15.52**	7.23	0.71	527	164	**137**	15	**1072**	54	27	**15**	87.2	110.1	21.8	92.9	17.7	4.2	19.5	2.9	15.0	2.7	6.9	0.9	4.6	0.7	387.1	329.7	57.4
		7.70	39.32	13.14	1.91	256	411	**349**	35	**950**	80	51	41	206.3	218.5	43.5	177.4	31.6	6.7	30.3	3.9	18.4	3.3	9.1	1.2	7.2	1.2	758.7	677.3	81.4
		5.12	51.09	28.72	2.50	452	244	37	44	225	76	68	52	114.0	230.9	28.4	106.7	19.8	4.2	17.3	2.9	16.4	3.3	9.7	1.4	9.1	1.4	565.5	499.8	65.8
		2.24	48.78	33.17	2.44	452	288	41	47	158	73	73	55	129.3	325.4	31.5	117.2	21.0	4.4	17.5	2.8	15.3	3.1	9.1	1.3	8.6	1.3	687.6	624.3	63.3
		3.34	53.22	24.70	2.62	513	406	**119**	48	253	68	51	60	135.2	392.8	39.1	149.7	27.9	5.6	21.8	2.9	13.7	2.5	7.3	1.1	7.4	1.2	808.0	744.7	63.3
		3.64	42.55	**40.84**	2.20	636	465	51	40	416	67	83	50	146.7	320.5	33.3	126.4	22.6	4.7	18.9	2.9	15.9	3.0	9.1	1.4	8.8	1.4	715.7	649.5	66.2
		4.49	50.04	29.99	2.44	499	341	46	45	354	**109**	69	56	125.9	233.8	29.6	109.5	20.8	4.6	21.2	3.3	19.0	3.8	10.9	1.5	9.8	1.5	595.1	519.6	75.5
		3.53	51.44	30.27	2.54	472	316	41	45	276	72	67	56	125.4	390.9	34.3	125.4	23.6	4.8	18.5	2.8	16.2	2.9	8.5	1.3	8.9	1.3	764.8	699.7	65.1
		4.06	55.74	24.28	2.62	479	285	40	48	201	82	55	59	134.7	280.0	31.5	111.6	21.1	4.5	18.2	2.7	15.0	2.9	8.5	1.4	8.9	1.3	642.4	579.0	63.4
		3.21	52.37	25.08	2.50	547	264	40	43	188	74	58	56	116.7	251.3	27.9	102.5	19.2	4.1	17.0	2.6	14.6	2.9	8.3	1.3	8.5	1.2	577.9	517.5	60.4
		3.13	56.17	24.87	2.65	547	246	35	47	189	75	58	60	125.2	270.9	29.2	106.9	18.9	4.0	16.2	2.5	14.7	2.9	8.5	1.4	9.0	1.3	611.6	551.1	60.5
		3.58	54.65	25.47	2.53	411	229	35	45	188	73	56	59	113.9	242.0	26.5	97.6	18.0	3.9	15.4	2.4	13.6	2.7	8.1	1.3	8.2	1.2	554.7	498.0	56.7
		5.34	53.79	24.98	2.56	411	234	40	45	206	73	60	58	124.8	273.0	28.2	100.1	18.6	3.9	16.1	2.4	14.1	2.7	7.9	1.3	8.5	1.3	602.8	544.7	58.1
ABRUZZI	ORSELLO – AB subset[3]	5.88	50.98	27.55	2.55	319	547	28	45	181	74	60	60	139.3	224.4	27.2	101.0	17.5	3.7	15.7	2.4	14.1	2.8	8.3	1.3	8.4	1.3	567.2	509.3	57.9
		7.52	52.54	23.17	2.82	254	438	29	51	209	74	59	62	103.6	299.2	20.7	79.4	15.0	3.2	13.9	2.2	13.4	2.8	8.0	1.3	8.2	1.3	572.2	517.9	54.3
		4.54	54.72	24.96	2.81	332	493	32	50	196	73	61	61	127.6	321.4	32.3	121.3	23.1	4.8	17.6	2.8	15.8	3.0	8.9	1.4	9.3	1.4	690.6	625.7	64.8
		7.55	53.38	22.82	2.68	281	547	36	46	212	62	58	59	78.8	207.6	18.3	66.1	14.0	3.0	11.9	2.1	13.0	2.6	8.0	1.3	8.8	1.4	436.9	384.9	52.0
		9.42	55.91	17.63	2.79	256	520	41	48	284	55	53	61	66.8	134.5	14.8	54.4	11.0	2.5	9.6	1.8	11.7	2.4	7.7	1.2	8.2	1.3	327.9	281.5	46.4
		8.28	52.44	23.13	2.66	287	458	45	47	271	61	60	60	106.7	313.8	27.2	93.0	18.1	3.6	12.9	2.3	13.3	2.7	7.8	1.3	8.6	1.4	612.7	558.8	53.9
SARDINIA	NURRA – SN subset[6]	**27.28**	38.69	16.68	2.18	637	474	66	50	215	**104**	64	45	209.0	380.0	nd	131.0	24.8	5.4	nd	nd	nd	nd	nd	3.0	10.2	1.5	764.9	744.8	20.1
		11.01	52.15	18.82	2.74	**877**	638	**75**	66	226	**143**	81	64	292.0	**585.0**	nd	222.0	44.9	9.8	nd	nd	nd	nd	nd	4.9	15.1	2.3	**1176.0**	**1143.9**	32.1
		2.13	64.01	15.53	3.43	822	729	54	68	184	**123**	73	71	644.0	**1470.0**	nd	604.0	117.0	25.5	nd	nd	nd	nd	nd	9.2	15.8	2.3	**2887.8**	**2835.0**	52.8
		nd	68.81	12.34	3.65	854	848	47	69	150	103	69	80	148.0	388.0	nd	175.0	40.1	8.9	nd	nd	nd	nd	nd	4.0	13.9	2.1	780.0	751.1	28.9
		6.70	68.86	5.41	3.38	693	776	21	63	108	66	50	77	26.4	82.0	nd	26.0	7.8	2.2	nd	nd	nd	nd	nd	1.5	10.7	1.6	158.2	142.2	16.0
		nd	75.73	4.94	3.88	750	847	17	80	101	83	46	**88**	27.9	60.0	nd	23.0	6.9	2.1	nd	nd	nd	nd	nd	1.5	12.3	1.9	135.6	117.8	17.8
		31.38	46.24	2.91	3.62	518	715	18	74	277	64	57	47	15.0	30.0	nd	11.0	4.3	1.4	nd	nd	nd	nd	nd	1.3	8.4	1.3	72.7	60.3	12.4
		43.58	36.43	**1.45**	2.62	188	256	6	60	187	55	31	**27**	63.0	98.0	nd	27.0	4.9	1.3	nd	nd	nd	nd	nd	1.1	6.2	1.0	202.5	192.9	9.6
		42.06	**21.89**	7.14	1.08	141	124	26	31	61	38	**16**	30	43.7	68.0	nd	31.0	6.6	1.6	nd	nd	nd	nd	nd	1.1	3.4	0.5	155.9	149.3	6.6
		38.97	**25.48**	15.72	1.22	216	177	74	32	119	91	26	32	133.0	182.0	nd	102.0	19.5	4.2	nd	nd	nd	nd	nd	1.9	6.3	1.0	449.9	436.5	13.4
		37.95	40.06	**1.66**	2.41	222	381	**3**	54	63	45	35	31	36.2	75.0	nd	26.0	4.2	1.1	nd	nd	nd	nd	nd	0.5	4.6	0.7	148.3	141.4	6.9
		19.42	49.39	13.92	2.95	499	543	37	66	103	75	49	60	34.3	89.0	nd	28.0	7.0	1.9	nd	nd	nd	nd	nd	1.7	8.4	1.3	171.6	158.3	13.3
		23.92	54.53	2.98	3.34	340	498	7	72	86	60	37	68	23.3	61.0	nd	17.0	4.2	1.2	nd	nd	nd	nd	nd	1.0	7.0	1.1	115.8	105.5	10.3
		26.63	52.70	**1.48**	3.70	331	358	**3**	77	133	57	27	56	10.6	24.0	nd	9.0	2.7	1.1	nd	nd	nd	nd	nd	1.0	6.5	1.0	55.9	46.3	9.6

(*continued on next page*)

Table 2 (*continued*)

Sampling site	Major oxides			Critical raw materials (CRMs)																									
	SiO_2 (wt.%)	Al_2O_3	Fe_2O_3	TiO_2 (ppm)	V	Cr	Co	Nb	Ni	Y	Sc	Ga	La (ppm)	Ce	Pr	Nd	Sm	Eu	Gd	Tb	Dy	Ho	Er	Tm	Yb	Lu	ΣREE	LREE	HREE
	12.00	64.68	3.79	3.92	449	583	**5**	76	60	60	42	76	15.5	34.0	nd	12.0	3.4	1.2	nd	nd	nd	nd	nd	1.2	7.1	1.1	75.5	64.9	10.6
Median	4.8	52.5	20.2	2.8	405.0	544.9	36.9	71.0	200.0	55.5	54.5	59.6	96.5	212.5	20.7	74.2	14.8	3.4	12.8	2.05	11.7	2.3	6.8	1.1	7.1	1.1	446.0	407.6	45.7
Min.	0.4	15.5	1.4	0.7	140.9	123.6	5.3	14.5	59.7	25.0	16.0	14.7	10.6	24.0	7.7	9.0	2.7	1.1	4.5	0.9	5.6	1.2	3.7	0.5	3.4	0.5	55.9	46.3	6.6
Max.	43.6	75.7	40.8	5.4	876.8	1130.0	348.9	129.0	1072.0	143.0	110.0	94.0	644.0	1470.0	55.3	604.0	117.0	25.5	30.3	4.0	20.6	3.8	10.9	9.2	15.8	2.3	2887.8	2835.0	85.9
Std.	9.2	9.8	7.6	0.9	156.9	269.1	40.7	26.3	165.5	18.4	14.4	11.9	74.6	199.7	9.1	64.4	12.3	2.7	4.7	0.6	3.0	0.5	1.4	0.9	1.9	0.3	343.2	335.6	16.6

1 = data from Mongelli et al., 2014; 2 = data from Mongelli et al., 2016; 3 = unpublished data; 4 = data from Mondillo et al., 2011; 5 = data from Boni et al., 2013; 6 = data from Mameli et al., 2007; nd = not detected; Min. = minimum value; Max. = maximum value; std. = standard deviation. Bold numbers indicate the outlier values.

those of either total REEs (median = 446, min = 56, max = 2888, std = 343) and LREE (median = 408, min = 46, max = 2835, std = 336) whereas the HREE show minor dispersion (median = 46, min = 6, max = 86, std = 16.6).

4.4. Multivariate statistics

An R-mode factor analysis was performed on the outliers-free database (n = 73) to evaluate interelemental relationships among major oxides and critical metals. Factors were extracted after Varimax rotation using the STATGRAPHICS Centurion XVI.I package. This operation was accomplished using a standardised correlation matrix, thereby weighting all the variables equally during factor calculations and using the classical method that replaces the diagonal elements with estimated communalities. The communalities provide an index of the efficiency of the proposed set of factors (Davis, 1986), and the magnitude of the communalities calculated in this study suggests that most of the original variance is still accounted for by the present set of factors.

Four factors explain 92.6% of the total variance in the geochemical database (Table 3). The first factor (F1; Var.% = 37.8) includes significant and positive weightings for TiO_2, Ni, and Nb and a negative weighting for Y. Ti and Nb share very similar geochemical behaviour and are largely insoluble under intense weathering conditions. These elements usually covary in karst bauxites as their distribution is mostly controlled by dry climate conditions promoting accumulation (Mongelli et al., 2016). The Ni^{2+} solubility in the metal–O–H system under mildly alkaline to acidic conditions throughout the whole Eh range keeps the ion available for adsorption onto secondary minerals and the anatase heavy metals sorption capability is well established (e.g. Guixia et al., 2011 and references therein). This suggests that anatase, which is the most abundant and ubiquitous Ti-phase in all the considered bauxite subsets, can control most of the Ni deriving from the dissolution of primary minerals. Yttrium is generally retained to behave as the heavy REE, although the Y-Ho fractionation during the scavenging exerted by oxi-hydroxides in soil has been documented (Bau, 1999; Kawabe et al., 1999). The Y negative loading in F1 may thus indicate that the dissolved pool of the element is not hosted in Ti-rich phases and do not follow the REEs fate during bauxitization.

The second factor (F2) explains 23.1% of the total variance within the dataset, and has significant and positive weightings for V, Sc, and REEs, but significant and negative weighting for Cr. REEs in these karst bauxites may concentrate both in detrital zircon, monazite and xenotime crystals, and in secondary fluorocarbonates and phosphates (Mameli et al., 2007; Boni et al., 2013; Mongelli et al., 2014). Secondary REE-rich minerals, which are decidedly less abundant than the detrital REE-rich ones, usually host LREE and especially cerium and, as a response of particular events, are observed in just few outlier samples (e.g. Mongelli et al., 2014) not included in the multivariate statistic database. Sc is commonly associated to the REEs because of its chemical similarity and tendency to concentrate in the same deposits (e.g. Hedrick and Templeton, 1990). Thus, its covariance with the REEs is not surprising although trivalent scandium commonly co-occurs with Fe^{3+} (Brookins, 1988) suggesting that most of the Sc is hosted in detrital iron-rich minerals like titanomagnetite. Similarly to scandium, also vanadium minerals are generally rare because the typical V^{3+} oxidation state in the crust makes it geochemically very similar to Fe^{3+} suggesting most of the vanadium content in these karst bauxites is controlled by ubiquitous and detrital iron-rich minerals. As for chromium insoluble trivalent chromium is easily released into aqueous solution as Cr^{6+} in the supracrustal environment (e.g. Margiotta et al., 2012 and references therein). F2 therefore represents differences in behaviour

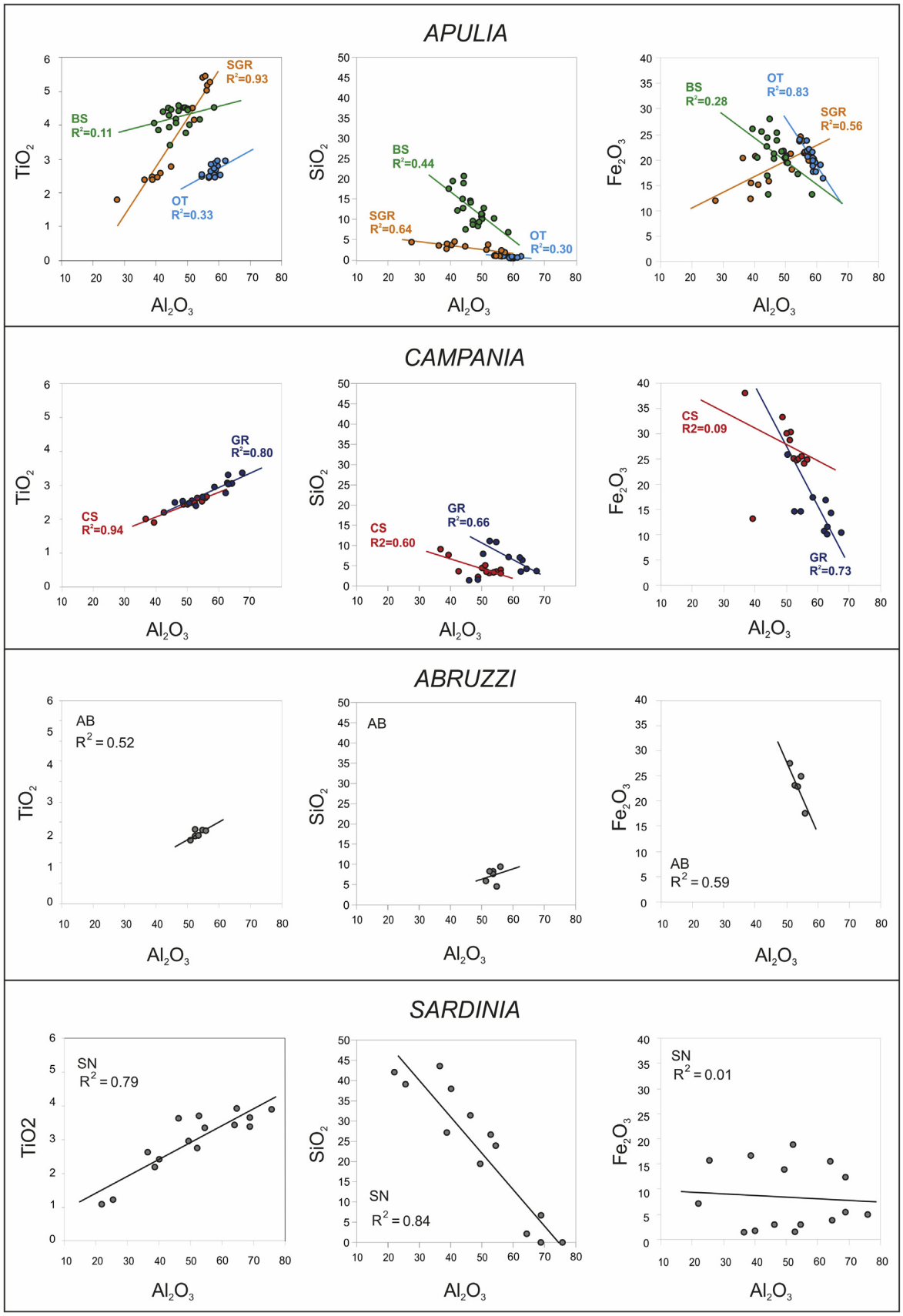

Fig. 2. Binary diagrams showing the relationships among the major oxides for each bauxite deposit. See the text for further details.

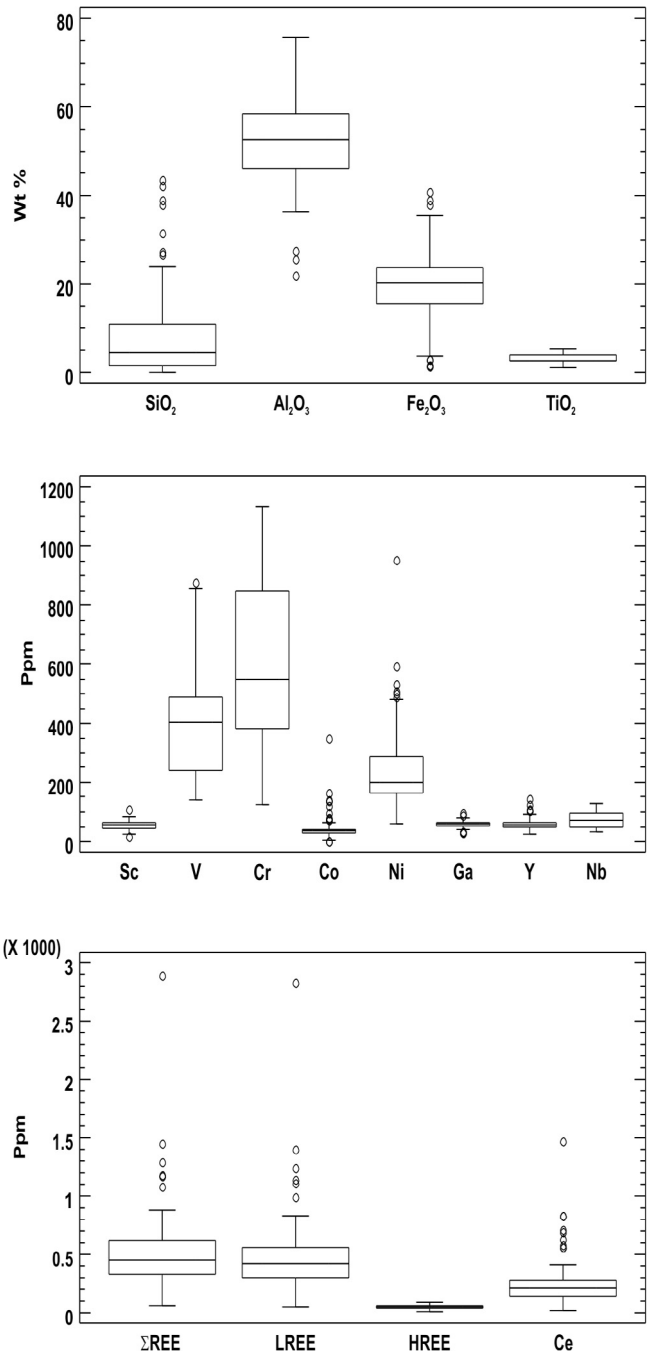

Fig. 3. Box and whisker plots for selected major and trace elements of all analyzed samples. The horizontal bar in the box refers to the median value; the ends of the whiskers are the maximum and minimum values of variables; the top and bottom of the boxes are the values of first and third quartiles; circles represent the outlier values of the dataset.

between trivalent largely insoluble metal cations such as REEs, Sc and V, hosted in detrital minerals, and chromium in surface environments.

The third factor (F3) explains 17.2% of the total variance within the dataset and has significant and positive weightings for Al_2O_3 and Ga. It is well known that gallium behaves the same way as aluminium and that bauxite can concentrate large amounts of the element (Schulte and Foley, 2013). Thus F3 represents the factor promoting the Al_2O_3 accumulation in karst bauxites, and also that of Ga one, which both occur during dry climatic conditions (e.g. Mongelli et al., 2014 and references therein).

Table 3
Results of the R-mode factor analysis after Varimax rotation.

	F1	F2	F3	F4
SiO_2				
Al_2O_3			0.90	
Fe_2O_3				0.78
TiO_2	0.80			
V		0.60		
Cr		−0.71		
Co				0.64
Nb	0.94			
Ni	0.82			
Y	−0.72			
Sc		0.77		
Ga			0.74	
ΣREE		0.61		
Var%	37.8	23.1	17.2	14.5

Note: Numbers are weights of the variables in the extracted factors. Variables having weight less than 0.60 are omitted.

The fourth factor (F4) includes significant and positive weights for Fe_2O_3 and Co. During bauxitization iron oxi-hydroxides forms under wetter climate whereas, during intense weathering, the Co^{2+} solubility in the metal–O–H system under mildly alkaline to acidic conditions throughout the whole Eh range is well established (Gaillardet et al., 2003). Consequently, Co is available for adsorption onto secondary minerals (e.g. Smith, 1999). Thus, the Fe_2O_3-Co covariance observed in F4 represents the capability of iron oxi-hydroxide to control Co through adsorption mechanism.

4.5. The significance of the outliers

As previously stated, outliers may reveal specific mineralisation events. Among the critical metals Co, and at a lesser extent Ni, are those showing the highest number of outliers, usually ranging well above the maximum value (Fig. 3, Table 2). In the nine Co-outliers samples, usually ranging above the maximum value, a correlation having a certain degree of significance with Ni ($r = 0.64$, $p < 0.1$) is observed. Co and Ni are considered a geochemical pair and, in some cases, may concentrate in weathering products forming under tropical climatic conditions (Berger et al., 2011). Bárdossy (1982), for instance, reported in karst bauxites the occurrence of bravoite from which Ni and Co migrated outward, toward the oxidized zone of the pristine mineral. Thus, in the Co-outliers the metal may be hosted in Ni-rich phases, likely concentrating in the pool of minerals occurring in the lateritic profile (Herrington et al., 2016).

Also the LREE distribution is characterized by the occurrence of several outliers clearly evidencing the Ce dispersion. Among the LREE association in karst bauxite, Ce fractionation is commonly observed (e.g. Mongelli et al., 2014). Due to its low ionisation potential, Ce behaves differently from the other REEs; therefore, highly variable positive cerium anomalies can be observed in karst bauxite deposits (McLennan, 1989) as a consequence of its peculiar redox chemistry. The Ce-outliers are distributed in several subsets (BS, SGR, GR and SN), where authigenic carbonate-fluoride and phosphate Ce-rich minerals have been detected (Mameli et al., 2007; Boni et al., 2013; Mongelli et al., 2014). Consequently, the LREE outliers are indicative of the processes promoting cerium accumulation in specific bauxite levels, and for this reason can be profitably used during the exploration stage.

It is interesting to observe that HREE have no outliers whereas yttrium, which is usually associated with the heavy rare earth elements, shows instead some outliers. The samples where these outliers are recorded can be observed in the SN subset. This suggests that yttrium can be affected by low temperature hydrothermal

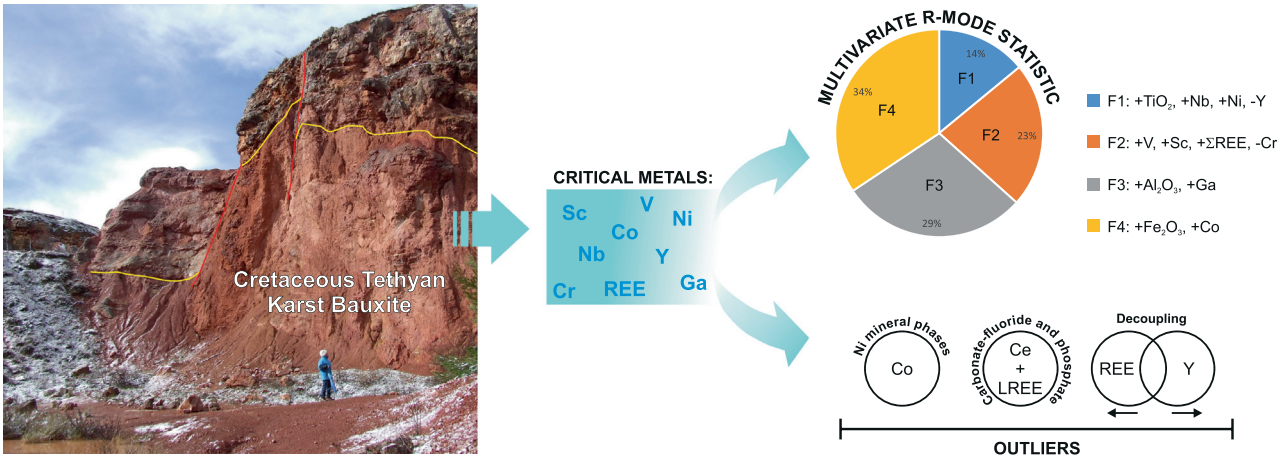

Fig. 4. Schematic representation of results of multivariate R-mode factor analysis and significance of outliers of Tethyan karst bauxites from Italy.

events, like those interfering with the bauxites of the Nurra district in Sardinia (Mameli et al., 2007).

5. Conclusions

In the karst bauxites of southern Italy and Sardinia Al-minerals mostly form at the expense of kaolinite after silica leaching under tropical climate promoting also TiO_2 accumulation whereas extreme wet climate favour the formation of iron phases. Re-silification processes, due to Tertiary hydrothermal events, can occasionally occur, like those affecting the Sardinian bauxite. Re-silification events in the Sardinian bauxite are clearly associated to the silica outliers thus demonstrating the effectiveness of univariate statistics in unroofing specific mineralisation events. Univariate statistics also indicate that some critical metals, especially Co, Ni, and LREE, have a significant number of outliers. The Co-Ni relationship associated to the outliers suggests that Co is likely hosted in Ni-rich phases whereas Ce accumulation in authigenic minerals, carbonate-fluoride and phosphate, is at the origin of LREE outliers (Fig. 4).

Multivariate R-mode statistics applied to the outliers-devoid database shows that most of the associated variance is explained by factors represented by simple element associations having positive loadings such as TiO_2-Nb, REEs-Sc-V, Al_2O_3-Ga, and Fe_2O_3-Co. This suggests that in absence of specific mineralization events, Al-, Fe-, and Ti-oxi-hydroxides plus detrital phases exert the main control on the distribution of most critical metals (Fig. 4). The fate of the critical metal Cr appears to be different from those of other critical trivalent and largely insoluble metals, being affected by a redox chemistry promoting its mobility as Cr^{6+}.

It has been observed that Y, whose behaviour usually mirrors that of the HREE, in the considered bauxites does not follow this behaviour in the outliers-devoid database, and has different outliers from those observed for the HREE. This behaviour may suggest that, during bauxitization, Y may suffer a decoupling from the REEs pool (Fig. 4).

Acknowledgments

Authors wish to thank Dr. A. Piccolo Papa and Dr. F. Putzolu for their support during fieldwork and sampling of the Abruzzi bauxite. Authors are also very grateful to two reviewers and Editor in Chief (Prof. F. Pirajno) for their constructive comments and suggestions that improved final version of the manuscript.

References

Abedini, A., Calagari, A.A., 2014. REE geochemical characteristics of titanium-rich bauxites: the Permian Kanigorgeh horizon, NW Iran. Turk. J. Earth Sci. 23, 513–532.

Ahmadnejad, F., Vahabzadeh, B., Zamanian, H., Sameti M., Asadi, H., 2016. Mineralogy, Geochemistry and Mass Changes at the Mombi Bauxite Deposit, (SW Iran): Using Geochemical Characteristics of the Immobile Elements in Geophysical Research Abstracts, v. 18, EGU2016-11466.

Bárdossy, G., 1982. Karst Bauxites. Bauxite Deposits on Carbonate Rocks Dev. Econ. Geol. 14. Elsevier, Amsterdam, p. 441.

Bárdossy, G., Boni, M., Dall'Aglio, M., D'Argenio, B., Pantò, G., 1977. Bauxites of peninsular Italy. Composition, origin and geotectonic significance. (Gebr. Borntraeger) Monographic series on Mineral Deposits 15, 61.

Bau, M., 1999. Scavenging of dissolved yttrium and rare earths by precipitating iron oxyhydroxide: experimental evidence for Ce oxidation, Y-Ho fractionation, and lanthanide tetrad effect. Geochim. Cosmochim. Acta 63, 67–77.

Berger, V.I., Singer, D.A., Bliss, J.D., Moring, B.C., 2011. Ni-Co laterite deposits of the world; database and grade tonnage models, US Geological Survey Open-file report, pp. 2011–1058.

Boni, M., Reddy, S.M., Mondillo, N., Balassone, G., Taylor, R., 2012. A distant magmatic source for Cretaceous karst bauxites of southern Apennines (Italy), revealed through SHRIMP zircon age dating. Terra Nova 24, 326–332.

Boni, M., Rollinson, G., Mondillo, N., Balassone, G., Santoro, L., 2013. Quantitative mineralogical characterization of karst bauxite deposits in the Southern Apennines, Italy. Econ. Geol. 108, 813–833.

Buccione, R., Mongelli, G., Sinisi, R., Boni, M., 2016. Relationship between geometric parameters and compositional data: a new approach to karst bauxites exploration. J. Geochem. Explor. 169, 192–201.

Brookins, D.G., 1988. Eh–pH Diagrams for Geochemistry. Springer-Verlag, Berlin.

Carannante, G., D'Argenio, B., Ferreri, V., Simone, L., 1987. Cretaceous paleokarst of the Campanian Appennines from early diagenetic to late filling stage. A case history. Rend. Soc. Geol. It. 9, 251–256.

Carannante, G., Pugliese, A., Ruberti, D., Simone, L., Vigliotti, M., Vigorito, M., 2009. Evoluzione Cretacica di un settore della piattaforma apula da dati di sottosuolo e di affioramento (Appennino campano-molisano). Boll. Soc. Geol. It. 128, 3–31.

Chiocchini, M., Farinacci, A., Mancinelli, A., Molinari, V., Potetti, M., 1994. Biostratigrafia a foraminiferi, dasicladali e calpionelle delle successioni carbonatiche mesozoiche dell'Appennino centrale (Italia). In: Mancinelli, A. (Ed.), Biostratigrafia dell'Italia centrale. Studi Geol. Camerti, spec. publ., Camerino, pp. 9–129.

Combes, P.J., 1990. Typologie, cadre geodynamique et genese des bauxites francaises. Geodin. Acta 4, 91–109.

Combes, P.J., Oggiano, G., Temussi, I., 1993. Geodynamique des bauxites sardes, typologie, génese et controle paleotectonique. C. R. Acad. Sci. Ser. II 316, 403–409.

Crescenti, U., Vighi, L., 1964. Caratteristiche, genesi e stratigrafia dei depositi bauxitici cretacei del Gargano e delle Murge: cenni sulle argille con pisoliti del Salento (Puglia). Boll. Soc. Geol. It. 83, 285–338.

Crescenti, U., Vighi, L., 1970. Risultati delle ricerche eseguite sulle formazioni bauxitiche cretaciche del Casertano e del Matese, in Campania. Mem. Soc. Geol. It. 9, 401–434.

Davis, J.C., 1986. Statistics and Data Analysis in Geology. Kansas Geological Survey, Wiley.

Deady, É.A., Mouchos, E., Goodenough, K., Williamson, B.J., Wall, F., 2016. A review of the potential for rare-earth element resources from European red muds: examples from Seydişehir, Turkey and Parnassus-Giona, Greece. Mineral. Mag. 80, 43–61.

Esu, D., Girotti, O., 2010. The late Oligocene molluscan fauna from Otranto (Apulia, Southern Italy): an example of alternating freshwater, lagoonal and emerged environments. Palaeontology 53, 137–174.
Funiciello, R., Montone, P., Parotto, M., Salvini, F., Tozzi, M., 1991. Geodynamical evolution of an intra-orogenic foreland: the Apulia case history (Italy). Boll. Soc. Geol. It. 110, 419–425.
Gaillardet, J., Viers, J., Dupre, B., 2003. Trace elements in river waters. In: Drever, J.I. (Ed.), Treatise of Geochemistry. Elsevier-Pergamon, Oxford, pp. 225–272.
Gamaletsos, P.N., Godelitsas, A., Kasama, T., Church, N., Douvalis, A.P., Goettlicher, J., Steininger, R., Boubnov, A., Pontikes, Y., Tzamos, E., Bakas, T., Filippidis, A., 2017. Nano-mineralogy and -geochemistry of high-grade diasporic karst-type bauxite from Parnassos-Ghiona mines, Greece. Ore Geol. Rev. 84, 228–244.
Gamaletsos, P.N., Godelitsas, A., Mertzimekis, T.J., Göttlicher, J., Steininger, R., Xanthos, S., Berndt, J., Klemme, S., Kuzmin, A., Bárdossy, G., 2011. Thorium partitioning in Greek industrial bauxite investigated by Synchrotron radiation and laser-ablation techniques. Nucl. Instrum. Methods Phys. Res., Sect. B 269, 3067–3073.
Guixia, Z., Xilin, W., Xiaoli, T., Xiangke, W., 2011. Sorption of heavy metal ions from aqueous solutions: a review. Open Colloid Sci. J. 4, 19–31.
Handy, M.R., Schmid, S.M., Bousquet, R., Bernoulli, D., 2010. Reconciling plate-tectonic reconstructions of Alpine Tethys with the geological–geophysical record of spreading and subduction in the Alps. Earth Sci. Rev. 102, 121–158.
Hanilçi, N., 2013. Geological and geochemical evolution of the Bolkardağı bauxite deposits, Karaman, Turkey: transformation from shale to bauxite. J. Geochem. Explor. 133, 118–137.
Hedrick, J.B., Templeton, D.A., 1990. Rare-Earth Minerals and Metals in US Bureau of Mines and Minerals Yearbook 1989. Government Printing Office, Washington D. C., pp. 825–844.
Herrington, R., 2013. Road map to mineral supply. Nat. Geosci. 6, 892–894.
Herrington, R., Mondillo, N., Boni, M., Thorne, R., Tavlan, M., 2016. Bauxite and Nickel-cobalt Lateritic Deposits of the Tethyan Belt. Society of Economic Geologists, Inc. Special Publication 19, 349–387.
Karadağ, M.M., Küpeli, S., Arýk, F., Ayhan, A., Zedef, V., Döyen, A., 2009. Rare earth element (REE) geochemistry and genetic implications of the Mortaş bauxite deposit (Seydişehir/Konya—Southern Turkey). Chem. Erde-Geochem. 69, 143–159.
Kawabe, I., Ohta, A., Ishii, S., Tokumura, M., Miyauchi, K., 1999. REE partitioning between Fe-Mn oxyhydroxide precipitates and weakly acid NaCl solutions: convex tetrad effect and fractionation of Y and Sc from heavy lanthanides. Geochem. J. 33, 167–179.
Ling, K.Y., Zhua, X.Q., Tanga, H.S., Wanga, Z.G., Yanc, H.W., Hana, T., Chend, W.Y., 2015. Mineralogical characteristics of the karstic bauxite deposits in the Xiuwen ore belt, Central Guizhou Province, Southwest China. Ore Geol. Rev. 65, 84–96.
Mameli, P., Mongelli, G., Oggiano, G., Dinelli, E., 2007. Mineralogy and geochemistry of the Nurra bauxites (Western Sardinia): constraints for the conditions of the formation and parental affinity. Int. J. Earth Sci. 96, 887–902.
Margiotta, S., Mongelli, G., Summa, V., Paternoster, M., Fiore, S., 2012. Trace element distribution and Cr(VI) speciation in Ca-HCO_3 and Mg–HCO_3 spring waters from the northern sector of the Pollino massif, southern Italy. J. Geochem. Explor. 115, 1–12.
McLennan, S.M., 1989. Rare earth elements in sedimentary rocks: influence of provenance and sedimentary processes. In: Lipin, B.R., McKay, G.A. (Eds.), Geochemistry and Mineralogy of Rare Earth Elements. Mineralogical Society of America, Reviews in Mineralogy, vol. 21, pp. 166–225.
Mindszenty, A., D'Argenio, B., Aiello, G., 1995. Lithospheric bulges at regional unconformities. The case of Mesozoic-Tertiary in Apulia. Tectonophysics 252, 137–161.
Mondillo, N., Boni, M., Balassone, G., Rollinson, G., 2011. Karst bauxites in the Campania Apennines (southern Italy): a new approach. Period. Mineral. 80, 407–432.
Mondillo, N., Boni, M., Balassone, G., Piccolo Papa, A., Putzolu, F., Arfè, G., 2016. The Campo Felice and Monte Orsello bauxite occurrences (Abruzzi, Italy), in Abstract 88° Congresso della Società Geologica Italiana, Napoli 7–9 Settembre 2016.
Mongelli, G., 1997. Ce-anomalies in the textural components of Upper Cretaceous karst bauxites from the Apulian Carbonate Platform (southern Italy). Chem. Geol. 140, 69–79.
Mongelli, G., Acquafredda, P., 1999. Ferruginous concretions in a Late Cretaceous karst bauxite: composition and conditions of formation. Chem. Geol. 158, 315–320.
Mongelli, G., 2002. Growth of hematite and boehmite in concretions from ancient karst bauxite: clue for past climate. Catena 50, 43–51.
Mongelli, G., Boni, M., Buccione, R., Sinisi, R., 2014. Geochemistry of the Apulian karst bauxites (southern Italy): chemical fractionation and parental affinities. Ore Geol. Rev. 63, 9–21.
Mongelli, G., Buccione, R., Sinisi, R., 2015. Genesis of autochthonous and allochthonous Apulian karst bauxites (Southern Italy): climate constraints. Sed. Geol. 325, 168–176.
Mongelli, G., Buccione, R., Gueguen, E., Langone, A., Sinisi, R., 2016. Geochemistry of the Apulian allochthonous karst bauxite, Southern Italy: distribution of critical elements and constraints on Late Cretaceous Peri-Tethyan palaeogeography. Ore Geol. Rev. 77, 246–259.
Muchos, E., Wall, F., Williamson, B.J., Palumbo-Roe, B., 2016. Easily leachable rare earth element phases in the Parnassus-Giona bauxite deposits, Greece, Bulletin of the Geological Society of Greece, vol. XLVIII – Proceedings of the 14th International Conference, At Thessaloniki, Greece.
Peh, Z., Kovačević Galović, E., 2014. Geochemistry of Istrian Lower Palaeogene bauxites: is it relevant to the extent of subaerial exposure during Cretaceous times? Ore Geol. Rev. 63, 296–306.
Oggiano, G., Sanna, G., Temussi, I., 1987. Caractères geologiques, litologiques et geochemiques de la bauxite de la Nurra. In: Cherchi, A. (Ed.), Livret-Guide Excursion en Sardaigne 24–29 Mai 1987. Groupe Francais du Crètacè, Cagliari, pp. 72–124.
Radusinovic, S., Jelenkovic, R., Pacevski, A., Simic, V., Bozovic, D., Holclajtner-Antunovic, I., Zivotic, D., 2017. Content and mode of occurrences of rare earth elements in the Zagrad karstic bauxite deposit (Niksic area, Montenegro). Ore Geol. Rev. 80, 406–428. http://dx.doi.org/10.1016/j.oregeorev.2016.05.026.
Reimann, C., Filzmoser, P., Garrett, R.G., 2002. Factor analysis applied to regional geochemical data: problems and possibilities. Appl. Geochem. 17, 185–206.
Schettino, A., Turco, E., 2011. Tectonic history of the western Tethys since the Late Triassic. Geol. Soc. Am. Bull. 123, 89–105.
Schulte R.F., Foley N.K. 2013. Compilation of Gallium resource data for Bauxite deposits, U.S. Department of the Interior, U.S. Geological Survey, Open-File Report 2013–1272, p. 14.
Smith, K.S., 1999. Metal Sorption on mineral surfaces: an overview with examples relating to mineral deposits. In: The Environmental Geochemistry of Mineral Deposits. Part A: Processes, Techniques, and Health Issues Volume Editors: Geoffrey S. Plumlee and Mark J. Logsdon, pp. 161–182.
Spalluto, L., 2012. Facies evolution and sequence chronostratigraphy of a mid-Cretaceous shallow-water carbonate succession of the Apulia Carbonate Platform from the Northern Murge area (Apulia, southern Italy). Facies 58, 17–36.
Tavani, S., Iannace, A., Mazzoli, S., Vitale, S., Parente, M., 2013. Late Cretaceous extensional tectonics in Adria: insights from soft-sediment deformation in the Sorrento Peninsula (southern Apennines). J. Geodyn. 68, 49–59.
Tavani, S., Vignaroli, G., Parente, M., 2015. Transverse versus longitudinal extension in the foredeep peripheral bulge system: role of Cretaceous structural inheritances during early Miocene extensional faulting in inner central Apennines belt. Tectonics 34, 1412–1430.
Vidal, O., Goffé, B., Arndt, N., 2013. Metals for a low-carbon society. Nat. Geosci. 6, 894–896.
Wang, Q., Deng, J., Liu, X., Zhang, Q., Sun, S., Jiang, C., Zhou, F., 2010. Discovery of the REE minerals and its geological significance in the Quyang bauxite deposit, West Guangxi, China. J. Asian Earth Sci. 39, 701–712.
Yu, W., Ruihu, W., Qilian, Z., Yuansheng, D., Yue, C., Yuping, L., 2014. Mineralogical and geochemical evolution of the Fusui bauxite deposit in Guangxi, South China: from the original Permian orebody to a Quarternary Salento-type deposit. J. Geochem. Explor. 146, 75–88.
Yuste, A., Bauluz, B., Mayayo, M.J., 2014. Genesis and mineral transformations in Lower Cretaceous karst bauxites (NE Spain): climatic influence and superimposed processes. Geol. J. http://dx.doi.org/10.1002/gj.2604.
Yuste, A., Bauluz, B., Mayayo, M.J., 2017. Origin and geochemical evolution from ferrallitized clays to karst bauxite: an example from the Lower Cretaceous of NE Spain. Ore Geol. Rev. 84, 67–79.
Zarasvandi, A., Charchi, A., Carranza, E.J.M., Alizadeh, B., 2008. Karst bauxite deposits in the Zagros Mountain Belt, Iran. Ore Geol. Rev. 34, 521–532.